

Boletim de Ciências Geodésicas

ISSN: 1413-4853 ISSN: 1982-2170

Universidade Federal do Paraná

Jesus, Janisson Batista de; Kuplich, Tatiana Mora; Barreto, Íkaro Daniel de Carvalho; Hillebrand, Fernando Luis; Rosa, Cristiano Niederauer da Speckle reduction for Sentinel-1A SAR images in the Semi-arid caatinga region, Brazil Boletim de Ciências Geodésicas, vol. 29, no. 3, e2023007, 2023 Universidade Federal do Paraná

DOI: https://doi.org/10.1590/s1982-21702023000300007

Available in: https://www.redalyc.org/articulo.oa?id=393976135002



Complete issue

More information about this article

Journal's webpage in redalyc.org



Scientific Information System Redalyc

Network of Scientific Journals from Latin America and the Caribbean, Spain and Portugal

Project academic non-profit, developed under the open access initiative

ORIGINAL ARTICLE

Speckle reduction for Sentinel-1A SAR images in the Semi-arid caatinga region, Brazil

Janisson Batista de Jesus¹ - ORCID: 0000-0001-8372-5557

Tatiana Mora Kuplich² - ORCID: 0000-0003-0657-4024

Íkaro Daniel de Carvalho Barreto³ - ORCID: 0000-0001-7253-806X

Fernando Luis Hillebrand⁴ - ORCID: 0000-0002-0182-8526

Cristiano Niederauer da Rosa⁵- ORCID: 0000-0003-3693-4764

¹ Universidade Federal de Sergipe, Programa de Pós-Graduação em Recursos Hídricos, São Cristóvão - Sergipe, Brasil.

E-mail: janisson.eng@gmail.com

²Instituto Nacional de Pesquisas Espaciais, Coordenação Espacial do Sul, Santa Maria - Rio Grande do Sul, Brasil. E-mail: tatiana.kuplich@inpe.br

³Centro Brasileiro de Pesquisa em Avaliação e Seleção e de Promoção de Eventos - CEBRASPE, Coordenação de Processamento de Dados e Resultados - CPDR, Brasília - DF, Brasil.

E-mail: daniel.carvalho.ib@gmail.com

Instituto Federal de Educação, Ciência e Tecnologia do Rio Grande do Sul, Departamento de Ensino,
Rolante - Rio Grande do Sul, Brasil.

E-mail: fernando.hillebrand@rolante.ifrs.edu.br

⁵Imagem Geosistemas, Soluções, São José dos Campos – São Paulo, Brasil.

E-mail: cristianonrd@gmail.com

Received in 7th September 2022. Accepted in 24th September 2023.

Abstract:

Due to the absence of studies related to the digital processing of synthetic aperture radar (SAR) images in the semi-arid region of Brazil, the aim of this study was to test different filters for reducing speckle noise in SAR images, serving as a reference for choosing the most suitable filter for different studies in this vegetation. The filters: Gamma Map, Lee Sigma, Median, Frost and Refined Lee in different window sizes were tested on the VV, VH and VH/VV polarizations in the Sentinel-1A images, verifying the responses under the influence of the dry and post-rainy period in the Caatinga vegetation. In the state of Sergipe, Brazil, 30 samples of Caatinga fragments obtained from Sentinel-1A images for the dry and post-rainy season were selected. For all images evaluated, the values of the averages of the equivalent number of looks (ENL) were compared by the Tukey test at 5% significance. The Gamma filter showed the highest amount of means (22) with the highest ENL values, followed by Median (5). The generation of ENL results and their comparison, considering all variables used, was essential to serve as a basis for choosing the filtering method in studies that use data from Sentinel-1A in the Caatinga region.

Keywords: Digital image processing; Noise; Synthetic aperture radar; Tropical dry forest.

How to cite this article: JESUS JB, KUPLICH TM, BARRETO IDC, HILLEBRAND FL, ROSA CN. Speckle reduction for Sentinel-1A SAR images in the Semi-arid caatinga region, Brazil. *Bulletin of Geodetic Sciences*. 29(3): e2023007, 2023.



This content is licensed under a Creative Commons Attribution 4.0 International License.

1. Introduction

The acquisition of images by the synthetic aperture radar (SAR) is carried out by transmitting and receiving coherent signals in the microwave range. The signals are formed by amplitude and phase in a complex number and each resolution cell of the radar image is the result of the contributions of all individual scatterers present in the cell. These contributions interfere in a destructive and constructive manner, resulting in speckle - a type of random noise intrinsic of this image type (Gleich 2018; Singh and Shree 2018). Speckle causes the typical granular appearance of SAR images, due to strong variations of phase interferences from pixel to pixel (Jideshi and Balaji 2018; Shafiei, Beheshti and Yazdian 2018).

Speckle reduces the visual quality of SAR images and can hamper their interpretation, affecting the accuracy of their classification and analysis (Gui, Xue, and Li, 2018; Torres et al. 2014). Therefore, one important step in the processing and, subsequently, analysis of SAR images consists of reducing the speckle effect before the extraction of the desired information (Lang, Yang and Li, 2015; Meng et al. 2018; Yue, Xu and Jin 2018). The filtering methods are prepared according to algorithms that are based on the speckle statistics and can be grouped in the frequency (wavelet) and spatial domains (Shafiei, Beheshti and Yazdian 2018; Yue, Xu and Jin 2018; Sivaranjani, Roomi and Senthilarasi 2019). Both are widely used, although spatial filters, such as mean and median filters, stand out for being simpler. Nevertheless, they are influenced, for instance, by the number of looks and window size applied to the image (Tang, Zhang and Ding 2019), and although there are a number of filters available, the selection of the window size is a challenging step in digitally processing images in order to choose the most suitable one (Mahdavi et al. 2018).

One of the ways to assess the level of speckle reduction can be through the analysis of the equivalent number of looks (ENL) that a given filter or window size generates in the resulting image. ENL allows a simple and general measurement of the speckle reduction applied in homogeneous areas, making it possible to compare the performance of different filters (Gleich 2018; Singh and Shree 2018; Liu, Zhang and Soon 2017; Mahdianpari et al. 2019) and its application does not require prior knowledge about the noiseless data (Jain and Ray 2019). However, the ENL is dependent on the size of the analyzed area in the image and as it is applied in homogeneous regions, the use in the entire image can generate high values, which must be observed regarding its use. As a way to reduce this problem, it should be evaluated using block processing in a non-overlapping fashion since the SAR image has a uniform and no uniform regions both (Singh and Shree 2018).

In Brazil, filter tests for speckle reduction in different window size configurations are still scarce to serve as pre-processing information for SAR images. Specifically in the semi-arid region of Brazil, this type of study does not yet exist. This region is composed of typical vegetation called Caatinga, also known as Tropical Dry Forest (FAO 2012). It occupies about 11% of the national territory, distributed across 10 states (MMA 2020). Therefore, the purpose of this study was to test different speckle filters using different window sizes in the Sentinel-1A C band images with VV, VH and the VH/VV band ratio in the Caatinga region. SAR images from dry and post-rainy periods were evaluated. The aim is also to generate data in order to serve as an information database in the pre-processing stage of these types of images in future studies that approach the Caatinga as a subject of study. Part of the content of this article is based on Jesus (2022).

2. Material and Methods

2.1 Study area

The studied region is located in the Alto Sertão Sergipano Territory, with an area of approximately 4,900 km² (Sergipe 2011, 2012), specifically in the municipalities of Canindé de São Francisco, Poço Redondo, and Porto

da Folha, in the state of Sergipe. It has a semi-arid climate of low latitude and altitude, classified as BSh according to the Köppen classification (Alvares et al. 2014). The soil is classified as a Luvisol and Planosol (Embrapa 2011) comprised in reliefs dissected in hills and tabular interflows, with a pediplain surface located in the Sertão Pediplain (Sergipe 2012).

The area presents a vegetal formation composed of deciduous trees and thorny shrubs, typical of semi-arid to arid climates (Veloso, Rangel-Filho and Lima 1991), characterized as hyper-xerophilous Caatinga (Ribeiro and Mello 2007). This vegetation was the focus of the study, where 30 remaining fragments distributed in the region were selected (Figure 1). To do this, a previous identification of the areas was carried out using optical images from Sentinel-2 and the Google Earth platform, and later on field visits, where they were verified and georeferenced by the absolute method, using the C/A code Global Navigation Satellite System (GNSS) from the Garmin GPSMap brand (from December 2018 to February 2019).

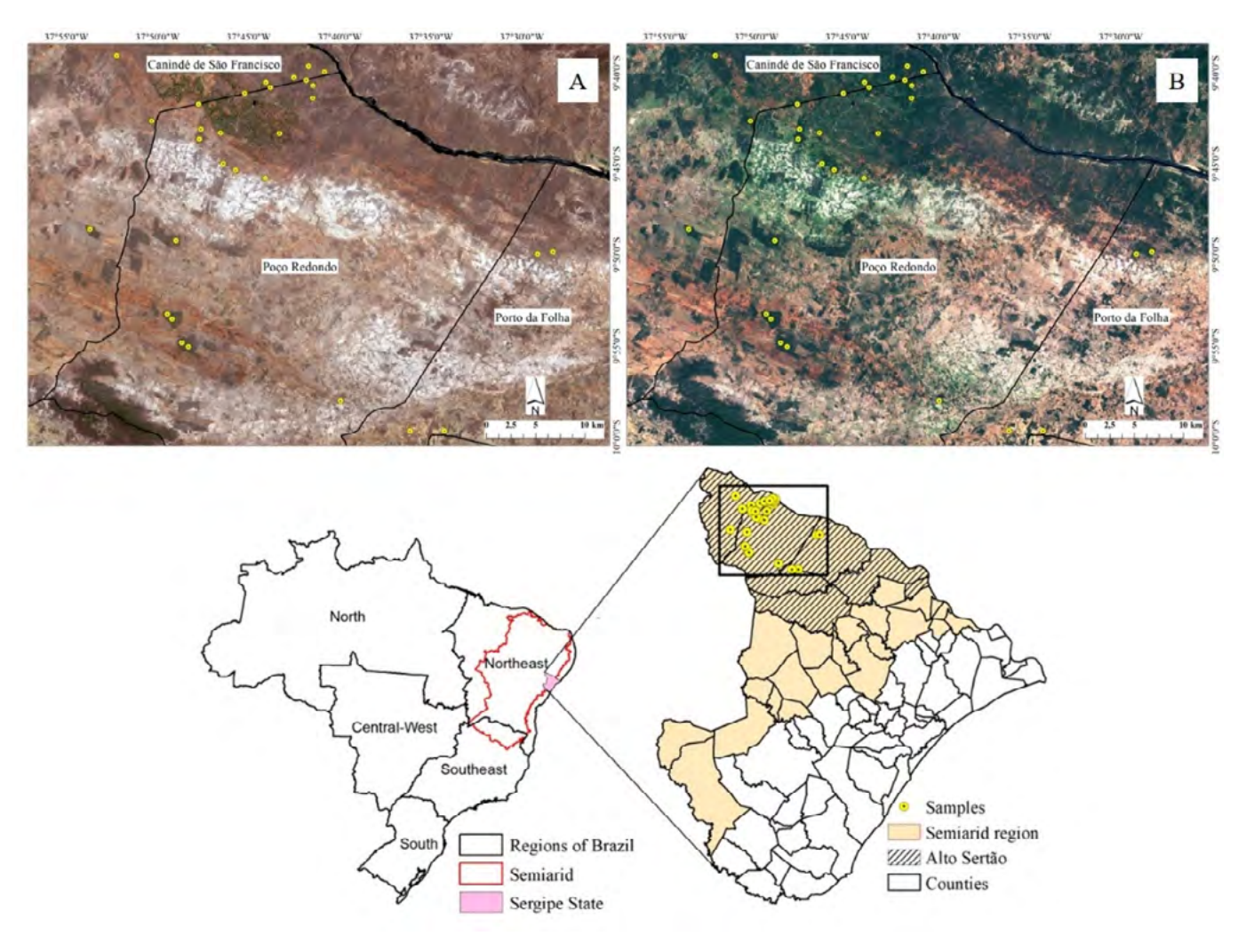


Figure 1: Location of the study area and sample Caatinga fragments selected and identified in the Sentinel-2 images in true color R4G3B2 (obtained during the dry season (A): 10/28/2018, and post-rainy period (B): 12/27/2018).

2.2 Data collection, processing and analysis

Sentinel-1A images were obtained in the VV and VH polarizations, in Interferometric Wide (IW) mode and level 1 Ground Range Detected (GRD) format (ESA 2019). Based on the polarized images, the band-ratio image through the relationship between cross- and co-polarization (VH/VV) for each period studied. The image acquisition dates were 10/26/2018 and 12/25/2018, referring, respectively, to the dry and post-rainy season (a condition in which there is no more occurrence of precipitation, but there is a canopy in the Caatinga) and based on the contrast of the physiological expression of vegetation in the region studied from the Normalized Difference Vegetation Index (NDVI) value according to data from the Moderate Resolution Imaging Spectroradiometer (MODIS) selected for the area of 250 x 250 m from the Caatinga (central coordinate: 9.70729 S; 37.68646 W) made available by the Web tool SATVeg (Embrapa 2019).

The rainfall condition (Station identification: 31785) obtained from the records of the historical database of the Integrated Environmental Data System of the National Institute for Space Research (INPE 2020) was also analyzed, in order to characterize the condition of the region studied. The precipitation event closest to the acquired images occurred for the dry period, 4 days before with a precipitated volume of only 8.5 mm/day, thereby not affecting the characteristics to be studied.

The pre-processing of the images was performed according to Filipponi (2019), and, as it was the case in their processing, the Sentinel Application Platform (SNAP) software (ESA 2020) was used. The tested filters were Gamma Map, Lee Sigma (both with 1 look), Median and Frost (this one with a damping factor of 2), applied in window sizes of 5 x 5, 7 x 7, 9 x 9, 11 x 11, and 15 x 15 pixels, Refined Lee and the image without filter (No Filter), in the VV and VH polarization and band ratio (VH/VV), calculated from the two previously filtered polarizations. The backscattering coefficients converted into decibels (dB) were extracted in each of the 30 samples selected in the Caatinga fragments, in a standardized manner, using a vector polygon in the same size shapefile format (area of 50 x 50 m), for each type of filter and window size applied, the whole process being carried out in both polarizations and in the band ratio, considering the two periods evaluated.

The evaluation of speckle smoothing was performed by calculating the ENL, which is widely used in studies with a focus on evaluating the reduction of this type of noise in homogeneous regions in SAR images (Gleich 2018; Singh and Shree 2018; Yue, Xu and Jin 2018; Jain and Ray 2019; Liu, Zhang and Soon 2017; Mahdianpari et al. 2019). The ENL value was obtained in each of the 30 samples selected from the Caatinga fragments for each filter and window size, in the three types of images (VV, VH, and VH/VV), analyzed in both periods (dry and post-rainy), and having the means compared using the Tukey test at the 5% significance level. All statistical analysis of the data was performed using the R software (R Core Team 2020).

3. Results

The mean ENL values between the filters in the windows analyzed for the dry period showed increasing values in all polarizations as the size of the applied window increased, with the exception of the Gamma and Lee Sigma filter between the 5 x 5 and 7 x 7 window in VH (Table 1). Additionally, a high standard deviation value was observed, mostly with results higher than the average obtained. Conversely, it is noted that the standard deviations were almost half of the mean value for the image without filter application and in the VH and VV polarizations. Considering the three polarizations studied, Gamma had the highest number (10) of mean values with the highest values compared to the other filters, followed by Median (4), which stood out with the highest number (7) when analyzing the second highest value between the results.

Table 1: Comparisons between mean ENL values for filters and window sizes (W) evaluated in the polarizations (Pol) studied for the dry period.

| Pol | w | No Filter | Filters | | | | | |
|-----------------|-----------|-------------|-------------------|----------------|---------------------|---------------------|-------------|--|
| | | | Frost | Gamma | Lee Sigma | Median | Refined Lee | |
| - - VH | No Filter | 92,3 (44,1) | А | А | А | А | | |
| | 5 x 5 | | 1003,8 A,B | 2041,8 A | 2013,4 A,B | 1048,3 A | 405,6 | |
| | | | (1197,9) | (5964,1) | (5974,1) | (1048,2) | (349,1) | |
| | 7 x 7 | | 2557,9 A,B,C | 1889,7 A | 1708,9 A,B | 2076,7 A | 405,6 | |
| | | | (5139,6) | (2673,9) | (2522,2) | (3241,3) | (349,1) | |
| | 9 x 9 | | 3545,3 b B,C | 3754,4 b A | 2912,6 a,b A,B | 3357,4 b A | 405,6 ª | |
| | | | (6230,8) | (3764,2) | (3105) | (3285,9) | (349,1) | |
| | 11 x 11 | | 4332,1 b B,C | 5665,4 b A | 4824,8 b B,C | 5961,8 b A | 405,6 ª | |
| - | | | (5385,5) | (4945,1) | (5034,5) | (5497,9) | (349,1) | |
| | 15 x 15 | | 5046,4 a,b C | 17126,1 cB | 9393,6 b,c C | 16486,1 ¢B | 405,6 ª | |
| | | | (5183,6) | (16646,7) | (12659,5) | (18146,3) | (349,1) | |
| VV . | No Filter | 44,8 (23,4) | А | А | Α | А | | |
| | 5 x 5 | | 353 b A,B | 416,2 b A | 376,7 b A,B | 373,7 b A,B | 162,6 ª | |
| | | | (261,2) | (312,8) | (336,5) | (246,8) | (110,4) | |
| | 7 x 7 | | 860,3 b A,B | 999,5 b A | 865,7 b A,B | 870,9 b A,B | 162,6 ª | |
| | | | (1006,6) | (1097,1) | (1156,1) | (640,5) | (110,4) | |
| | 9 x 9 | | 1332,1 b A,B | 1785,9 b A,B | 1437,7 b A,B | 2029,7 ь а,в | 162,6 ª | |
| | | | (1483,5) | (1393) | (1448,9) | (1832,3) | (110,4) | |
| | 11 x 11 | | 1897,2 a,b B,C | 4810,3 a,b B,C | 3188,1 b B | 5722,8 ь в,с | 162,6 ª | |
| | | | (2308,8) | (6919,2) | (3382,5) | (9986,6) | (110,4) | |
| | 15 x 15 | | 3172,4 a,b C | 8248,5 b,c C | 6162,5 a,b,c C | 9676 °C | 162,6 a | |
| | | | (5029,9) | (9410,1) | (8846) | (14767) | (110,4) | |
| - VH/VV - | No Filter | 3 (3,3) | A | Α | Α | А | | |
| | 5 x 5 | | 13,9 b A,B | 16,3 b A | 13,4 a,b A | 12,8 a,b A | 5,8 a | |
| | | | (11,3) | (14,7) | (12,8) | (8,2) | (4,3) | |
| | 7 x 7 | | 23,5 b A,B | 33,4 b A,B | 24,5 b A | 29,6 b A,B | 5,8 a | |
| | | | (14,8) | (27,2) | (25,8) | (23,5) | (4,3) | |
| | 9 x 9 | | 38,2 b B,C | 59,2 b A,B | 44,8 b A,B | 56,5 b A,B | 5,8 a | |
| | | | (25) | (36,5) | (52,2) | (45,1) | (4,3) | |
| | 11 x 11 | | 54,7 a,b C | 113 cB | 71,7 ^{c B} | 106,8 b,c B | 5,8 a | |
| | | | (38,3) | (87,4) | (86,9) | (93,6) | (4,3) | |
| | 15 x 15 | | 88,3 a D | 311,1 bC | 133,2°C | 273,4 bC | 5,8 a | |
| | | | (82,1) | (298,8) | (112) | (264,2) | (4,3) | |

^{*} In parentheses: Standard Deviation. a, b, c: Different subgroups for the Tukey test between the filters. A, B, C, D: Different subgroups for the Tukey test between the applied windows.

The comparison of the mean values for the VH image indicated that there are no significant differences between the filters for the 5×5 and 7×7 windows, with even Gamma and Lee Sigma presenting higher values for the 5×5 windows, and Frost and Median presenting them for the 7×7 windows. In the 9×9 window, Lee Sigma showed statistical similarity with both Refined Lee and the other filters, which in turn had no significant difference between their mean values, with Gamma presenting the highest mean for this window. In the 11×11 window, there was a statistical difference only between Refined Lee and the other filters, with a higher average for Median,

followed by Gamma. In the 15 x 15 window, Gamma and Median stood out statistically with the highest averages. When comparing the statistical differences in the mean values between the window sizes in the filters, there was a similarity between Frost and Lee Sigma, as well as Gamma and Median, which they showed differences only between the 15×15 window and the other sizes.

In the VV image, it was noted that there is a significant difference only between the Refined Lee filter and the others for the 5×5 , 7×7 and 9×9 windows, with Gamma having the highest means for the first two and Median followed by Gamma for the abovementioned third window. The Median filter also stood out for the 11×11 and 15×15 windows, showing better results than the others. When analyzing the mean values between the windows in the filters, there is a similarity between the responses of the statistical test as the size of the windows increases, with emphasis on Gamma, which did not show similarity of the values in the 5×5 and 7×7 windows with the others.

The image resulting from the band ratio showed lower values when compared to the VH and VV polarizations. Additionally, it was found that the Gamma filter showed higher mean values in all applied windows. Statistically, Gamma and Frost stood out in the 5×5 window size. In the 7×7 and 9×9 windows, there was a statistical difference only between the Refined Lee filter and the others, with Gamma presenting the highest mean value for both windows. The same filter had the highest mean value also in the size of 11×11 , differing statistically from Refined Lee and Frost. In the 15×15 window, the respective highest mean values were seen in Gamma and Median, with statistical similarity between them. When comparing the results between the window sizes, there is a similarity between the statistical responses across the filters. The Frost filter had greater discrimination between the means in the windows, with the 15×15 differing from the others.

When analyzing the ENL averages for the post-rainy season, increasing values were observed for the filters in all polarizations as the size of the windows increased (Table 2). High standard deviations are also observed in the results obtained, with values above average, in particular for the Frost, Gamma and Lee filters Sigma in the 7 x 7 window in the VH polarization, which presented almost three times, in the case of the first one, and twice as much, in the last two, in relation to the average. Meanwhile, the standard deviations for the original images were lower than average, with the VH and VV presenting values close to half in relation to the average. Considering the three polarizations studied, Gamma had the highest number (12) of mean values with the highest values compared to the other filters, followed by Frost (2), with Lee Sigma being the filter with the highest number (5) considering the second highest value.

The statistical comparison in the VH polarization did not detect any difference between the mean ENL values for the 7 x 7 window. The statistical responses between the filters were similar for 5 x 5 and 15 x 15, the difference being verified only in Median for the largest window size, which was statistically different from Refined Lee. The same similarity between the statistical responses was seen in the 9×9 and 11×11 windows, but with the larger one showing a difference only between Refined Lee and all other filters. When analyzing the mean values between the windows by filter, there is similarity in the statistical responses in Gamma and Median, in which the size of 15×15 differs from the other windows.

The mean ENL values for the VV image indicated statistically equal responses between the filters for the 7 x 7 and 9 x 9 windows, with statistical difference only between Refined Lee and the others. The Gamma filter stood out both in the 5×5 window, with Lee Sigma being statistically equal, as in the 15×15 . When comparing the values of the mean values between the windows in the filters, an equal response is observed for Gamma and Lee Sigma, with statistical difference only between the 15×15 and the others. In this same window size, Median also had a difference in relation to all the others. In the Frost filter, there is one highlight: there is greater discrimination between the mean values along the window sizes, being the only one to present, in all results, Subgroup D, which is associated with the largest windows.

Table 2: Comparisons between mean ENL values for filters and window sizes (W) evaluated in the polarizations (Pol) studied for the post-rainy season.

| Pol | W | No Filter | Filters | | | | |
|-------|-----------|--------------|---------------------|--------------|--------------|----------------------|-------------|
| | | | Frost | Gamma | Lee Sigma | Median | Refined Lee |
| - | No Filter | 100,3 (52,8) | А | А | А | А | |
| | 5 x 5 | | 885,2 a,b A | 1105,7 b A | 1036,8 b A | 716,1 a,b A | 367 ª |
| | | | (875,3) | (1090,5) | (1127,6) | (649,7) | (235) |
| | 7 x 7 | | 3442,4 A | 4434,1 A,B | 4035,3 A | 2126,3 A,B | 367 |
| VH . | | | (9089,4) | (8615,9) | (8617,3) | (1947,3) | (235) |
| | 9 x 9 | | 4466 b A,B,C | 6118,5 b A,B | 5146,7 b A | 3484 a,b A,B | 367 a |
| _ | | | (5602) | (7085,7) | (5566,3) | (2730,3) | (235) |
| | 11 x 11 | | 5218,8 b B,C | 6140,3 ыв | 6015,6 b A | 6412,6 bB | 367 a |
| | | | (4542,8) | (5877,4) | (6366,4) | (6687,1) | (235) |
| | 15 x 15 | | 7686,7 a,b C | 16765,6 bc | 14018,8 ьв | 15057,2 bC | 367 a |
| | | | (8544,1) | (14516,8) | (19257,4) | (16431,6) | (235) |
| | No Filter | 36,9 (15,3) | Α | Α | Α | Α | |
| - | 5 x 5 | | 440,5 a,b A,B | 552,1 bA | 499,6 6 4 | 462,6 a,b A,B | 148,4ª |
| | | | (419,1) | (590,9) | (554,1) | (460,3) | (96,2) |
| - | 7 x 7 | | 848,2 b A,B,C | 864,4 bA | 748,7 b A | 758 b A,B | 148,4 a |
| | | | (731,2) | (609,1) | (623,5) | (569,7) | (96,2) |
| VV | 9 x 9 | | 1240,1 b в,с | 1330,7 b A | 1197,2 b A | 1205,4 b A,B | 148,4ª |
| | | | (1233,5) | (1327,3) | (1378,6) | (1025,7) | (96,2) |
| | 11 x 11 | | 1685,4 b C,D | 2097,6 b A | 1809,8 b A | 2063,9 ^{bB} | 148,4ª |
| | | | (1641,9) | (2303,7) | (2310,8) | (2516,3) | (96,2) |
| | 15 x 15 | | 2848,3 a,b D | 6487,8 c B | 4477,3 b,c B | 5058,9 b,c C | 148,4ª |
| | | | (3143,3) | (7819,4) | (6152,1) | (4583,3) | (96,2) |
| | No Filter | 3,1 (2,6) | Α | Α | Α | Α | |
| - | 5 x 5 | | 21,5 b A,B | 26,3 b A | 22,8 b A | 19,9 a,b A | 7,5 ª |
| VH/VV | | | (20,6) | (23,8) | (22,4) | (15,5) | (5,7) |
| | 7 x 7 | | 58,2 b A,B,C | 75,3 b A | 55,5 b A,B | 57,9 b A,B | 7,5 a |
| | | | (64,3) | (85,1) | (68,1) | (55,2) | (5,7) |
| | 9 x 9 | | 101,9 ь в,с | 76,8 b A | 66,2 a,b A,B | 72,5 b A,B | 7,5 ª |
| _ | | | (167,5) | (64,8) | (68,5) | (63,5) | (5,7) |
| | 11 x 11 | | 130,2 b C | 145,6 bA | 104,9 a,b B | 121,2 ы в | 7,5 a |
| | | | (201,8) | (197,4) | (140,3) | (122) | (5,7) |
| | 15 x 15 | | 143,8 a,b C | 423,1 c B | 197,9 a,b C | 290,3 b,c C | 7,5 a |
| | | | (146,6) | (479,5) | (201,5) | (266,1) | (5,7) |

^{*} In parentheses: Standard Deviation. a, b, c: Different subgroups for the Tukey test between the filters. A, B, C, D: Different subgroups for the Tukey test between the applied windows.

In the image of the band ratio, the responses of the statistical comparison are similar between the 9 x 9 and 11 x 11 windows, with differences only between Refined Lee and the other filters. There is also a similarity between 5 x 5 and 7 x 7, with a difference in the statistical responses found only in the Median filter, where the smallest window has a statistically similar mean value between Refined Lee and the other filters, while in the 7 x 7, there is statistical equality between all filters except for Refined Lee. In the 15 x 15 window size, the high mean value verified in Gamma conditioned the highlight among the filters used, being followed only by Median. When

analyzing the comparison between the windows in each filter, it is observed that Lee Sigma and Median have the same statistical response, with the 15 x 15 window differed from the others. The same was observed in the Gamma filter, although the other window sizes were statistically equal to each other. Frost draws attention for presenting statistical similarity in the largest Subgroup (C) in the windows ranging from 7×7 to 15×15 .

When analyzing the descriptive statistics through the boxplots of the studied images referring to the dry period (Figure 2), a general pattern in the distribution of the ENL values of the filters is noticed for the different window sizes and polarizations, with an increasing curve until Median and later decrease until the image without filter (No Filter), which becomes more accentuated as the size of the windows increases. It is also observed that the Gamma and Median filters have their values of 1st quartile, median and 3rd quartile above the other filters, presenting their boxes, which contain 50% of the data, superior to the others. The ENL values obtained in the VH polarization are slightly higher than in VV, with a marked difference of these for the VH/VV for the dry period (Figure 2a), with Refined Lee and the image without filter having the lowest values in all responses. The Median filter showed the highest ENL values for the 3rd quartile in general, followed by Gamma, although it also presented a great amplitude between the quartiles, mainly in the 5 x 5 window in the VH polarization, as well as 15 x 15 in the VV. Nevertheless, Gamma also had a high amplitude in the boxplot, mainly in the 9 x 9 and 11 x 11 windows for VH and VV, and in the 15 x 15 dimension for the latter polarization. Also, considering the amplitude between the quartiles, Lee Sigma was the filter with the longest distance between the 1st and 3rd quartiles and with the largest amount of outliers in the 15 x 15 window of the VH image.

In the post-rainy season, the distribution of the ENL values of the filters in the different window sizes and polarizations has, in general, a standard upward curve to Median and a subsequent decrease to No Filter, being much more characterized as the size of the windows (Figure 2b). In general, the Gamma and Median filters stand out among the others, having their values in the 1st quartile, median and 3rd quartile above the other filters, thereby presenting their boxes, which contain 50% of the data, higher to the others.

The highest ENL values observed in the boxplots for the data of the post-rainy period are seen in the image with the VH polarization, followed by the VV and the VH/VV image, in which a more pronounced reduction is verified for all sizes of windows. The Lee Sigma filter showed high values for the 3^{rd} quartile in VH images, surpassing even Gamma in the 9×9 and 11×11 windows. Lee Sigma, however, demonstrated high amplitudes between the 1^{st} and 3^{rd} quartiles between the analyzed filters, with a smaller variation in the VH and VV polarization in the 1^{st} windows, having the largest amount of outliers in these same images. The image without filter is notably the one with the lowest ENL values in all windows and polarizations, followed by Refined Lee.

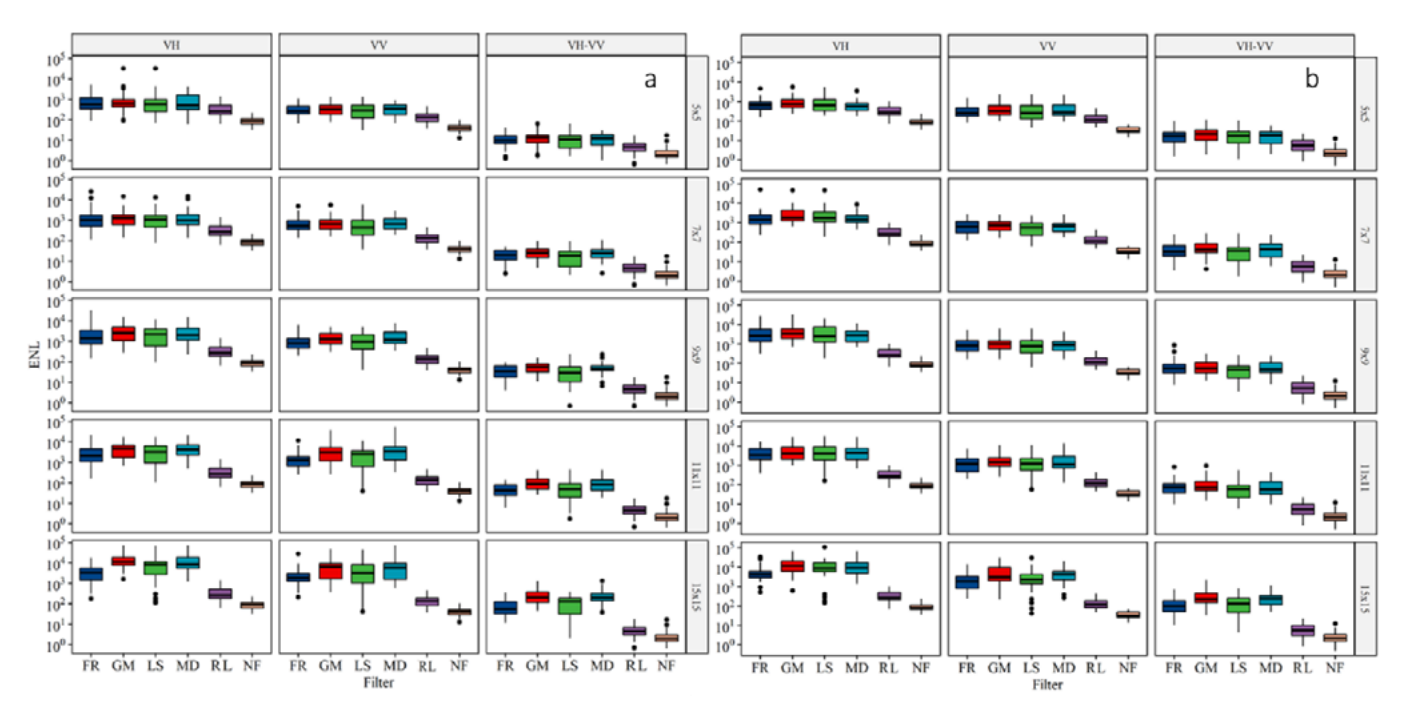


Figure 2: Boxplots of descriptive statistics of the filters and original image (FR: Frost; GM: Gamma; LS: Lee Sigma; MD: Median; RL: Refined Lee; NF: No Filter), windows (5 x 5; 7 x 7; 9 x 9; 11 x 11;15 x 15) and polarization (VH; VV; VH/VV) for Caatinga samples referring to the dry period (a) and post-rainy (b). The box refers to the 1st quartile, median, and 3rd quartile. The points are outliers.

The filtering step reduced the noise present in the images for each type of data used and in each evaluated period. This smoothing can be visually noticed in Figure 3, where the most prominent filter in speckle smoothing (mainly in VH polarization) is compared to the original image.

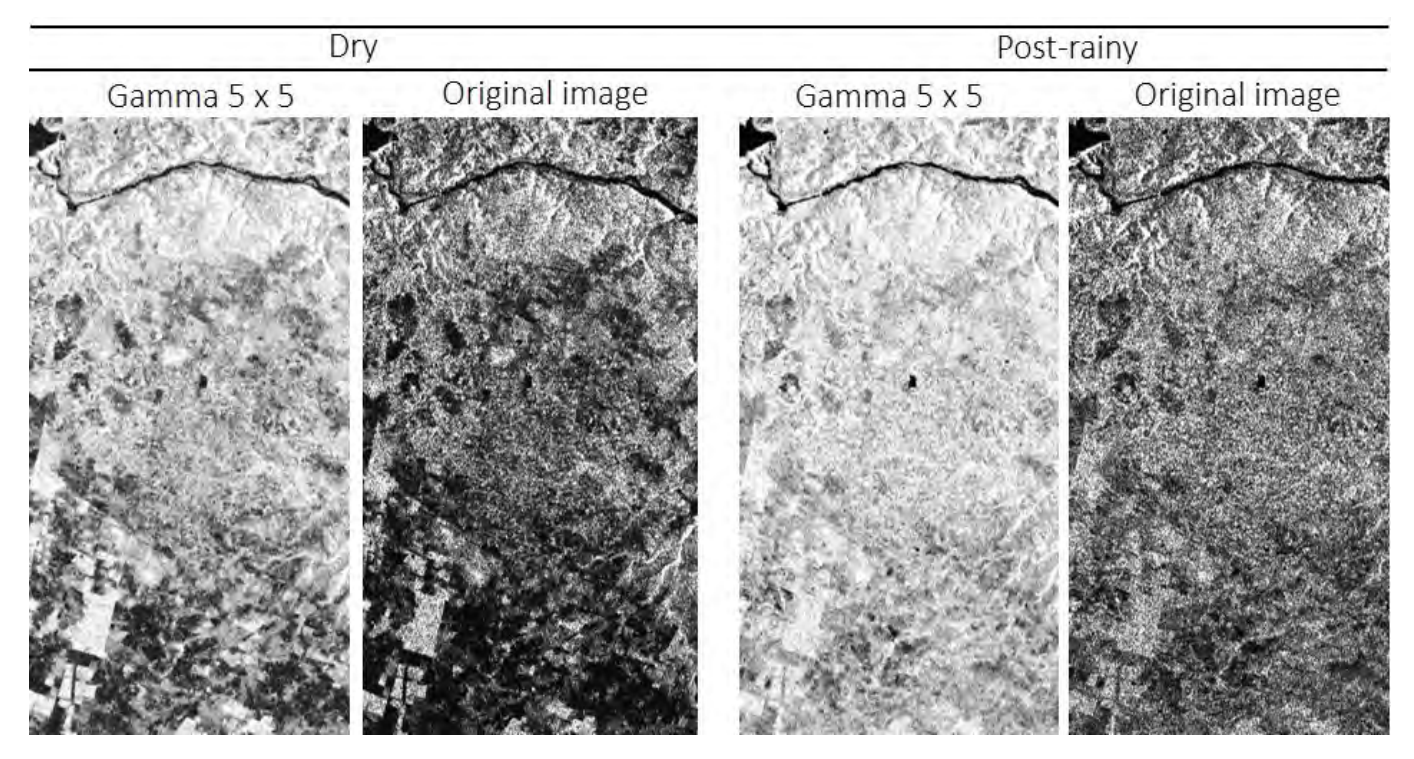


Figure 3: Visual representation of the VH polarization for the dry and post-rainy period after the Gamma filter in the 5 x 5 pixel window and the image without filtering application.

4. Discussion

The application of ENL as the main index for evaluating noise attenuation capacity in homogeneous areas in SAR images (Zhang et al. 2019) showed that the smoothing capacity is influenced by the type of filter, polarization, window size, and vigor condition of the Caatinga. It was common to observe the high standard deviations among all the answers found, which hindered the statistical discrimination between the compared means. This high variation in relation to the average indicates the great variability of the pixel values within this type of vegetation, reflecting the different structures of the Caatinga, as the SAR signal varies according to the types of vegetation (Ottinger and Kuenzer 2020).

Despite the current abundance of Sentinel-1 data and the availability of tools for their processing and analysis, the occurrence of deforestation in the Caatinga resulting from human intervention makes the analysis of multitemporal filtering of images a challenge, since deforestation can happen anytime and, consequently, alter the samples selected for statistical analysis. As rainy and dry seasons directly affect the landscape of the studied region, when comparing the periods of the evaluated images, it is observed that the Caatinga vigor condition affects the ENL responses, denoting varied pixel values for this vegetation, whether green or dry. This is related to the SAR signal resulting from the deciduous characteristics of this plant typology (Cole 1960), which occurred during the typical period of low water supply in the semi-arid region (Carmo and Lima 2020), allowing greater penetration of the radar signal into the vegetation. In turn, in times of greater rainfall, the Caatinga presents a large canopy cover with leaves, which hinders or prevents the penetration of the radar signal, considering that the Sentinel-1A data are obtained from the C band, which has its ability to penetrate up to a few centimeters into the plant canopy (Ottinger and Kuenzer 2020).

Thus, the SAR signal (represented by the pixel values after ENL) for the dry period is more related to the internal structures of the Caatinga, such as branches and trunks, mainly as a consequence of the double-bounce spread. For the post-rainy season, the SAR signal is the result of the interaction with the components of the canopy that generate volumetric spreading (Freeman and Durden 1998). Therefore, the ENL results obtained for the Caatinga are also associated with its vigor state and the type of polarization of the signal emitted and how it interacts with vegetation.

As the ENL values were higher for the VH image considering the results for each period, it indicates that there is a greater attenuation of noise in the cross polarization for the filters and windows used, which may imply that there is less variation between the value of pixels in this type of image. A relationship between this polarization and aboveground biomass in tropical forests is observed from Sentinel-1A data (Ananto et al. 2019).

Nevertheless, when comparing the VV polarization in the analyzed periods, it is observed that there is less variation between the pixel values for the dry season of the Caatinga, as there is a greater ENL value for the image without filtering treatment. It presents even higher mean values in this vegetation condition when compared to the moment of vigor also for the studied filters. Such a response may be related to the interaction of this co-polarization with vertical structures, a consequence of the greater penetration of the microwave due to the absence of a canopy (Henderson and Lewis 1998). In addition to the influence of the condition of the vegetation, the choice of filters that reduce the noise of SAR images is also an important factor for each polarization, as verified for the modeling of the biomass of homogeneous pastures in Envisat ASAR images, that Frost is the most suitable filter for VH polarization, while the Lee filter is the most suitable for the VV polarization (Wang, Ge and Li 2012).

In this study, the Gamma filter stood out with the highest number of mean values superior to the others analyzed, being the filter with the greatest capacity to reduce speckle noise. The high performance of this spatial filter may be related to higher power spectral density after the suppression of the high-frequency multiplicative speckle (HMS) noise when compared to other filters such as Frost and Lee Sigma (Shahrezaei and Kim 2019). In addition to the Gamma filter, Median also stood out as the second to present the largest number of mean values

with the highest ENL values. Both also had relevance for the greater number of the second highest mean values. These results with high speckle smoothing power are justified when analyzing the descriptive statistics for both the dry and post-rainy periods, as these filters generally presented their values of 1st quartile, median and 3rd quartile above other filters.

Despite the gamma filter having excelled in speckle smoothing in the present study, it is observed that in other studies it did not present the same response. This could be related to the type of polarization and radar band used, as in the study by Tang, Zhang and Ding (2019), where they used TerraSAR-X image, showing opposite results between different filters for standard deviation, peak signal-to-noise ratio (PNSR) (the higher the value, the more efficient the de-speckling performance, with an image of superior quality) and ENL, being that Gamma presented greater standard deviation, lower ENL and lower PSNR, showing inferior performance over the Median filter, as well as Frost, which was also evaluated in his study. The Gamma filter also did not excel in speckle smoothing when using the L band for ALOS-PALSAR (HH and HV) and JERS-1 SAR (HH) images when compared to Frost, which presented higher ENL values and lower Speckle Suppression Index (SSI) values for Frost, indicating better performance for noise reduction (Shamsoddini and Trinder 2012). However, the same authors used ERS-2 SAR (VV) images as did Mahdavi et al. (2018) from Radarsat-2 which use C-band sensor, the same band as Sentinel-1, and even so the Gamma filter did not show greater speckle smoothing. This may be related to the landscape elements that make up the analyzed image.

It is also noteworthy that the composition of the landscape of the studied region has a strong contrast, mainly with areas of exposed soil resulting from human activity and pasture that differ from areas of Caatinga, mainly of dense character, which can also interfere in the responses of the speckle and its smoothing. In the dry season, this entire landscape is modified, and even the Caatinga areas appear to be degraded (but that is the evolutionary condition of the vegetation), however the pasture also stands out, being totally exposed soil. That is, there is a variation in the spatial landscape in each period and when each period is compared.

Two other factors also influence the speckle reduction capacity: the damping factor within a fixed window and the size of the windows. The damping factor allows you to define the level of smoothing of the filter used, with lower damping values resulting in greater smoothing while higher values edges preserve better but smooth less. Larger windows can generate excessive smoothing while smaller ones can maintain a lot of noise (Tabassum, Vaccari and Acton 2018), since, as seen in the observed results, larger window sizes provide higher ENL values and a greater reduction in speckle.

As expected, the increase in ENL was observed as the window size increased, with the 15 x 15 window being the greatest ability to reduce speckle noise. The influence of different filters (Frost, Gamma map, Lee Sigma, Lee, Boxcar and Median) under 3 x 3 and 5 x 5 windows was also verified by Rana and Suryanarayana (2019) using Sentinel-1 images, noting the influence the size of windows in speckle smoothing. Therefore, in addition to the type of filter, the analysis of the window size is relevant as they change the results of the analyzes as in the mapping and classification of land use and land cover studies (Shitole et al. 2015). The influence of window sizes was also observed by Woźniak et al. (2016) on ALOS/PALSAR L-band images under different spatial window sizes and decomposition windows (3 x 3, 5 x 5, 7 x 7 and 9 x 9 pixels) and polarimetric decomposition methods, and by Pavanelli et al. (2018) when comparing the speckle reduction capability of Lee and Frost filters by testing 3 x 3, 5 x 5, 7 x 7, 9 x 9, 11 x 11, and 13 x 13 window sizes using ALOS/PALSAR- 2. Using the C-band of the Radarsat-2 satellite, Idol, Haack and Mahabir (2017) using the HH and HV polarization and the Lee Sigma filter, the 5 x 5 window presented better accuracy values when compared to 3 x 3. However, when performing the classification using texture data in the measurements of 5 x 5, 9 x 9, 13 x 13 and 17 x 17 of this same filtering method, the accuracy was lower than the original image, indicating that the smoothing caused by the filter reduced the image texture measures for land use and land cover classification. This situation occurs because the texture adds additional information to the classification process. Therefore, it is important to analyze the influence of different window sizes on each type of data to be analyzed.

5. Conclusions

The study made it possible to compare the responses of the ENL and, subsequently, the attenuation of the speckle, associating the different window sizes for each filter in each type of polarization and period of the Sentinel-1A image, discriminating statistical differences between the results for Caatinga vegetation.

The Gamma filter was the most representative in terms of the number of highest average values for the ENL, being indicated to attenuate the speckle in the studied Caatinga. The study allowed us to verify the filters that provide less speckle attenuation, which can serve as a basis of choice for studies with Sentinel-1 in the studied Caatinga that do not want a greater speckle reduction effect.

Additionally, although this study is a pioneer in testing the different responses in the filtering process using radar data for the Caatinga biome, it should be noted that the biome presents different physiognomies. So, in caatingas with another composition and vegetal structure, it is necessary to carry out another evaluation for the variables analyzed. Therefore, the specific filter must be chosen according to the window, polarization and time of the image (condition of the vegetation) to be used associated with the objective of the study. And given that Sentinel-1 is a satellite that provides free images and that there is a tendency for it to be widely used, this study serves as a basis for future studies with this type of data in Caatinga vegetation.

ACKNOWLEDGMENTS

The authors would like to thank the financial support provided by the Coordination for the Improvement of Higher Education Personnel (CAPES), Brazil, for the development of this research.

AUTHOR'S CONTRIBUTION

Author1: Conceptualization, literature review, methodology, writing; Author2: Writing – revision, final approval; Author3: Data analysis; Author4: Data collection; Author5: Data collection.

REFERENCES

Alvares, C.A., et al 2014. Köppen's climate classification map for Brazil. Meteorologische Zeitschrift, 22(6), pp.711-728.

Ananto, W. H. G., et al 2019. Performance of various speckle filter methods in modelling forest aboveground biomass using Sentinel-1 data: case study of Barru Regency, South Sulawesi. In: *Sixth Geoinformation Science Symposium*. Yogyakarta, Indonesia, 2019, Bellingham: Proceedings.

Carmo, M. V. N. S and Lima, C. H. R. 2020. Caracterização espaço-temporal das secas no Nordeste a partir da análise do índice SPI. *Revista Brasileira de Meteorologia*, 35(2), pp.233-242.

Cole, M. M. 1960. Cerrado, Caatinga and Pantanal: the distribution and origin of the savanna vegetation of Brazil. *The Geographical Journal*, 126(2), pp.168-179.

Embrapa. 2019. *SATVeg*. Sistema de análise temporal da vegetação. Available at:< https://www.satveg.cnptia. embrapa.br/satveg/login.html> [Accessed 2 January 2019].

Embrapa. 2011. *Sistema brasileiro de classificação de solos*. **Solos brasileiros**. **Mapa de solos do Brasil. Escala: 1:5.000.000**. **Available at:**https://www.embrapa.br/tema-solos-brasileiros/solos-do-brasil [Accessed 20 January 2020].

ESA. 2019. European Space Agency. Copernicus Open Access Hub. Available at:https://scihub.copernicus.eu/ [Accessed 2 January 2019].

ESA. 2020. European Space Agency. SNAP Download. Available at:http://step.esa.int/main/download/snap-download/ [Accessed 5 September 2020].

FAO. 2012. Food and Agriculture Organization of the United Nations. *Global ecological zones for FAO forest reporting*: 2010 Update. Forest Resources Assessment. Rome, working paper 179.

Filipponi F. 2019. Sentinel-1 GRD Preprocessing Workflow. Proceedings, 18(1), pp.1-11.

Freeman, A. and Durden, S. L. 1998. A three component scattering model for polarimetric SAR data. *IEEE Transactions Geoscience Remote Sensing*, 36, pp.963-973.

Gleich, D. 2018. Optimal-dual-based l_1 analysis for speckle reduction of SAR data. *IEEE Transactions Geoscience Remote Sensing*, 56(11), pp.6674-6685.

Gui, Y., Xue, L. and Li, X. 2018. SAR image despeckling using a dilated densely connected network. *Remote Sensing Letters*, 9(9): 857-866.

Henderson, F. M. and Lewis, A. J. 1998. *Manual of remote sensing: principles and applications of imaging radar*. 3rd ed. New York: John Wiley Sons.

Idol, T., Haack, B. and Mahabir, R. 2017. Radar speckle reduction and derived texture measures for land cover/use classification: a case study. *Geocarto International*, 32(1), pp.18-29.

INPE. 2020. Instituto Nacional de Pesquisas Espaciais. *Sistema integrado de dados ambientais*. Available at:http://sinda.crn.inpe.br/PCD/SITE/novo/site/index.php> [Accessed 1 March 2020].

Jain, S. K. and Ray, R. K. 2019. Non-linear diffusion models for despeckling of images: achievements and future challenges. *IETE Technical Review*, 37(1), pp.66-82.

Jesus, J. B. 2022. Estimativa de biomassa acima do solo de caatinga através de imagens SAR. Tese (Doutorado em Sensoriamento Remoto). Programa de Pós-Graduação em Sensoriamento Remoto, Universidade Federal do Rio Grande do Sul (UFRGS), Porto Alegre/RS.

Jideshi, P. and Balaji, B. 2018. Adaptive non-local level-set model for despeckling and deblurring of synthetic aperture radar imagery. *International Journal of Remote Sensing*, 39(20), pp.6540-6556.

Lang, F., Yang, J. and Li, D. 2015. Adaptive-window polarimetric SAR image speckle filtering based on a homogeneity measurement. *IEEE Geoscience and Remote Sensing Letters*, 53(10), pp.5435-5446.

Liu, S., Zhang, G. and Soon, Y. T. 2017. An over-complete dictionary design based on GSR for SAR image despeckling. *IEEE Geoscience and Remote Sensing Letters*, 14(12), pp.2230-2234.

Mahdianpari, M., et al 2019. A Gaussian random field model for de-speckling of multi-polarized synthetic aperture radar data. Advances in Space Research, 64(1): 64-78.

Mahdavi, S. et al. 2018. Speckle filtering of synthetic aperture radar images using filters with object-size-adapted windows. *International Journal of Digital Earth*, **11(7)**, pp.703-729.

Meng, Y. et al. 2018. Adaptive pseudo-p-norm regularization based de-speckling of SAR images. *Remote Sensing Letters*, 9(12), pp.1177-1185.

MMA. 2020. Ministério do Meio Ambiente. Biomas. Caatinga. Available at:http://www.mma.gov.br/biomas/ Caatinga> [Accessed 10 August 2020].

Ottinger, M. and Kuenzer, C. 2020. Spaceborne L-band synthetic aperture radar data for geoscientific analyses in coastal land applications: a Review. *Remote Sensing*, 12(14), pp.2228.

Pavanelli, J. A. P., et al 2018. PALSAR-2/ALOS-2 and OLI/Landsat-8 data integration for land use and land cover mapping in Northern Brazilian Amazon. Boletim de Ciências Geodésicas, 24(2), pp.250-269.

R Core Team. 2020. *R: A Language and Environment for Statistical Computing*. R Foundation for Statistical Computing, Vienna, Austria.

Rana, V. K. and Suryanarayana, T. M. V. 2019. Evaluation of SAR speckle filter technique for inundation mapping. *Remote Sensing Applications: Society and Environment*, **16**, pp.100271.

Ribeiro, A.S. and Mello, A.A. 2007. *Diagnóstico da biota*. Estudos para criação do Monumento Natural Grota do Angico. Sergipe: Governo de Sergipe, Secretaria de Estado do Meio Ambiente e dos Recursos Hídricos.

Sergipe. 2012. Secretaria de Estado do Meio Ambiente e dos Recursos Hídricos. *Atlas Digital sobre Recursos Hídricos de Sergipe*. Sistema de informações sobre recursos hídricos de Sergipe. Aracaju: Superintendência de Recursos Hídricos do Estado de Sergipe.

Sergipe. 2011. Secretaria de Estado do Planejamento, Orçamento e Gestão de Sergipe. Aracaju: Superintendência de Estudos e Pesquisas.

Shafiei, A., Beheshti, M. and Yazdian, E. 2018. Distributed compressed sensing for despeckling of SAR images. *Digit Signal Processing*, 81, pp.138-154.

Shahrezaei, I. H. and Kim, H.-C. 2019. Resolutional analysis of multiplicative high-frequency speckle noise based on SAR spatial de-speckling filter implementation and selection. *Remote Sensing*, 11(9), pp.1041.

Shamsoddini, A. and Trinder, J.C. 2012. Edge-detection-based filter for SAR speckle noise reduction. *International Journal of Remote Sensing*, 33(7), pp.2296-2320.

Shitole, S., et al 2015. Selection of suitable window size for speckle reduction and deblurring using SOFM in polarimetric SAR images. *Journal of the Indian Society of Remote Sensing*, 43(4), pp.739-750.

Singh, P. and Shree, R. 2018. A new SAR image despeckling using directional smoothing filter and method noise thresholding. *International Journal of Engineering, Science and Technology*, 21(4), pp.589-610.

Sivaranjani, R., Roomi, M. M. and Senthilarasi, M. 2019. Speckle noise removal in SAR images using Multi-Objective PSO (MOPSO) algorithm. *Applied Soft Computing*, 76, pp.671-681.

Tabassum, N., Vaccari, A. and Acton, S. 2018. Speckle removal and change preservation by distance-driven anisotropic diffusion of synthetic aperture radar temporal stacks. *Digit Signal Processing*, 74, pp.43-55.

Tang, X., Zhang, L. and Ding, X. 2019. SAR image despeckling with a multilayer perceptron neural network. *International Journal of Digital Earth*, 12(3), pp.354-374.

Torres, L., et al 2014. Speckle reduction in polarimetric SAR imagery with stochastic distances and nonlocal means. *Pattern Recognition*, 47(1), pp.141-157.

Veloso, H. P., Rangel-Filho, A. L. R. and Lima, J. C. A. 1991. *Classificação da vegetação brasileira adaptada a um sistema universal*. Rio de Janeiro: IBGE.

Wang, X., Ge, L. and Li, X. 2012. Evaluation of filters for ENVISAT ASAR speckle suppression in pasture area. In: XXII ISPRS Congress, *ISPRS Annals of the Photogrammetry, Remote Sensing and Spatial Information Sciences*. Melbourne, Australia, 25 August - 01 September 2012.

Woźniak, E., et al 2016. The influence of filtration and decomposition window size on the threshold value and accuracy of land-cover classification of polarimetric SAR images. *International Journal of Remote Sensing*, 37(1), pp.212-228.

Yue, D.-X., Xu, F. and Jin, Y.-Q. 2018. SAR despeckling neural network with logarithmic convolutional product model. *International Journal of Remote Sensing*, 39(21), pp.7483-7505.

Zhang, G., et al 2019. Speckle Reduction by Directional Coherent Anisotropic Diffusion. Remote Sensing, 11(23), pp.2768.